Available online at www.sciencedirect.com
SCIENCE DIRECT®
Journal of Sound and Vibration 269 (2004) 511–534
JOURNAL OF SOUND AND VIBRATION
www.elsevier.com/locate/jsvi

Dynamic analysis of an arch due to a moving load

Jong-Shyong Wu*, Lieh-Kwang Chiang

Department of Naval Architecture and Marine Engineering, National Cheng-Kung University, Tainan, 701, Taiwan, ROC

Received 25 February 2002; accepted 2 January 2003

Abstract

The radial (in-plane) bending-vibration responses of a uniform circular arch under the action of a moving load were investigated by means of the arch (curved beam) elements. Instead of the complex explicit-form shape functions given by the existing literature, the simple implicit-form shape functions associated with the radial (normal), tangential and rotational displacements of the arch element were derived. Based on the relationships between the nodal forces and nodal displacements of an arch element the elemental stiffness matrix was obtained, and based on the equation relating the kinetic energy and nodal velocities the elemental consistent mass matrix was determined. Assembly of the elemental property matrices yields the overall stiffness and mass matrices of the complete circular arch. The analytical free vibration analysis results were used to confirm the reliability of the presented stiffness and mass matrices for the arch element. Then the dynamic responses of a typical segmental circular arch, with constant curvature, due to a concentrated load moving along the circumferential direction were discussed. In addition to the circular arch, a hybrid (curved) beam composed of a circular-arch segment and two identical straight-beam segments was also studied. All numerical results were compared with the finite element solutions based on the conventional straight-beam elements and reasonable agreement was achieved. Influence of the moving speed, centrifugal force and frictional force on the dynamic behaviors of the circular arch and the hybrid beam was investigated.

1. Introduction

For most structural engineers, how to choose a suitable finite element to perform the static or dynamic analysis of the curved structures, such as arches, rings, shells and railway bridges is still a difficult problem; thus a lot of investigators devoted themselves to this field. Since the present paper aims at the in-plane responses of the arch, only a little information regarding the out-of-

*Corresponding author. Fax: +886-6-280-8458.
E-mail address: jswu@mail.ncku.edu.tw (J.-S. Wu).

0022-460X/03/$ - see front matter © 2003 Elsevier Science Ltd. All rights reserved.
doi:10.1016/S0022-460X(03)00020-8

plane behavior of the curved beams was mentioned. In the existing literature, most of the researchers are interested in the derivations of displacement (or shape) functions and stiffness matrix of the arch elements [1–6], few of them paid attention to the derivations of the mass matrix of the arch elements [7–9]. For this reason, the literature about the static analysis of arches is much more than that about the dynamic analysis. As we know, Refs. [7–9] are the three papers most concerned. In Ref. [7], the first few natural frequencies and mode shapes of a small thin arch with three supporting conditions and various subtended angles were studied. In Ref. [9], the free vibrations of circular arches with various depths of cross-sections and various types of supports were investigated by taking account of the effects of rotary inertia and shear deformation. As to the engineering background of a curved beam under a moving load one may refer to the Introduction of Ref. [10]. To the authors' knowledge, the information regarding the forced vibration responses of an arch due to the moving load(s) is rare and this is the reason why this paper tries to study the title problem.

In Ref. [7], the elemental stiffness matrix and consistent mass matrix for the arch element were derived based on two "explicit-form" functions for the tangential and the radial displacements, where the displacement functions are the power series of curvilinear co-ordinates s and the effect of rotary inertia is neglected. In the recent papers [6,9], the 18 "explicit-form" shape functions for the tangential displacement, the radial displacement and the rotational angle, for an arch element, were derived and based on these shape functions the element stiffness matrix and mass matrix were obtained. Where the shape functions are the algebraic-trigonometric functions of the angular co-ordinate θ. Because the "explicit-form" shape functions and element property matrices presented in Refs. [6,7,9] are very complicated, this paper employs the simple "implicit-form" shape functions to derive the "implicit-form" element stiffness and mass matrices of the arch (curved beam) element with the effect of rotary inertia considered [11].

For comparisons, both the arch (curved beam) elements and straight-beam elements were used to solve the same problem. In addition to a uniform 120° circular arch, a hybrid beam composed of a circular-arch segment and two identical straight-beam segments was also studied. Since the velocity of moving load, V_P, the centrifugal force induced by the curvilinear motion of the moving load along the curved beam, F_c, and the frictional force between the moving load and the beam, F_f, are the key factors affecting the dynamic behaviors of the curved beams, the influence of these factors is discussed.

2. Shape functions

For the arch (curved beam) element shown in Fig. 1, if the x-axis is the symmetric axis for the cross-section of the arch and the effect of shear deformation is ignored, then the displacement functions for the radial displacement u_x, the circumferential displacement u_θ and the rotational angle ψ_y are given by [1]

$$u_x = G_1 + G_2 \cos\theta + G_3 \sin\theta + G_4\theta \sin\theta + G_6\theta \cos\theta, \tag{1a}$$

$$u_\theta = G_1 C\theta + G_2 \sin\theta - G_3 \cos\theta + G_4(\sin\theta - \theta\cos\theta) + G_5 + G_6(\cos\theta + \theta\sin\theta), \tag{1b}$$

$$\psi_y = G_1\left(\frac{C}{R}\right)\theta + G_4\left(\frac{2}{R}\right)\sin\theta + G_5\left(\frac{1}{R}\right) + G_6\left(\frac{2}{R}\right)\cos\theta, \tag{1c}$$

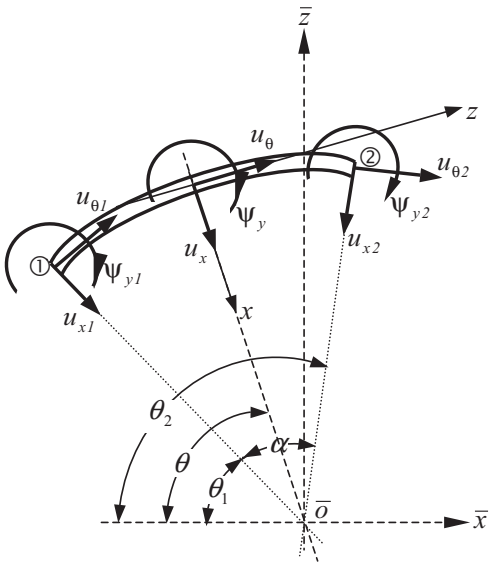

Fig. 1. The definition for the in-plane element displacements, u_x, u_θ and ψ_y, for an arch element and the associated reference local and global co-ordinate systems, xyz and $\overline{xyz}$.

where

$$C = 1 + (I_y/AR^2). \tag{2}$$

In Eqs. (1) $G_1 - G_6$ are the integration constants determined by the boundary conditions of the arch element, while in Eq. (2), A is the cross-sectional area, R is the average radius of curvature of the arch element and I_y is the moment of inertia of the area A about the y-axis given by [1]

$$I_y = \int_A \frac{x^2}{1-(x/R)}\,\mathrm{d}A. \tag{3}$$

In Fig. 1, xyz and $\overline{xyz}$ are the local and global reference co-ordinate systems for the conventional straight-beam elements, respectively.

In matrix form, Eqs. (1) gives

$$\{u\} = [H]\,\{G\}, \tag{4}$$

where

$$\{u\} = \begin{Bmatrix} u_x & u_\theta & \psi_y \end{Bmatrix}, \tag{5a}$$

$$[H] = \begin{bmatrix} 1 & \cos\theta & \sin\theta & \theta\sin\theta & 0 & \theta\cos\theta \\ C\theta & \sin\theta & -\cos\theta & \sin\theta - \cos\theta & 1 & \cos\theta + \theta\sin\theta \\ \frac{C}{R}\theta & 0 & 0 & \frac{2}{R}\sin\theta & \frac{1}{R} & \frac{2}{R}\cos\theta \end{bmatrix}, \tag{5b}$$

$$\{G\} = \begin{Bmatrix} G_1 & G_2 & G_3 & G_4 & G_5 & G_6 \end{Bmatrix}. \tag{5c}$$

In Eqs. (4) and (5), the symbols [] and {} represent the rectangular (or square) matrix and the column vector, respectively.

When the boundary conditions for the arch element shown in Fig. 1 are imposed on Eq. (4), one obtains

$$\{\delta\} = [B]\,\{G\}, \tag{6}$$

where

$$\{\delta\} = \{\, u_{x1} \quad u_{\theta 1} \quad \psi_{y1} \quad u_{x2} \quad u_{\theta 2} \quad \psi_{y2} \,\}, \tag{7}$$

$$[B] = \left[\begin{array}{ccc|ccc} 1 & \cos\theta_1 & \sin\theta_1 & \theta_1\sin\theta_1 & 0 & \theta_1\cos\theta_1 \\ C\theta_1 & \sin\theta_1 & -\cos\theta_1 & \sin\theta_1-\theta_1\cos\theta_1 & 1 & \cos\theta_1+\theta_1\sin\theta_1 \\ \frac{C}{R}\theta_1 & 0 & 0 & \frac{2}{R}\sin\theta_1 & \frac{1}{R} & \frac{2}{R}\cos\theta_1 \\ \hline 1 & \cos\theta_2 & \sin\theta_2 & \theta_2\sin\theta_2 & 0 & \theta_2\cos\theta_2 \\ C\theta_2 & \sin\theta_2 & -\cos\theta_2 & \sin\theta_2-\theta_2\cos\theta_2 & 1 & \cos\theta_2+\theta_2\sin\theta_2 \\ \frac{C}{R}\theta_2 & 0 & 0 & \frac{2}{R}\sin\theta_2 & \frac{1}{R} & \frac{2}{R}\cos\theta_2 \end{array}\right]. \tag{8}$$

From Eq. (6) one obtains

$$\{G\} = [B]^{-1}\{\delta\}. \tag{9}$$

The substitution of Eq. (9) into Eq. (4) yields

$$\{u\} = [N]\,\{\delta\}, \tag{10}$$

where $[N]$ is a matrix of the shape functions defined by

$$[N(\theta)] = [H]\,[B]^{-1} = \begin{bmatrix} N_{11}(\theta) & N_{12}(\theta) & \cdots & N_{16}(\theta) \\ N_{21}(\theta) & N_{22}(\theta) & \cdots & N_{26}(\theta) \\ N_{31}(\theta) & N_{32}(\theta) & \cdots & N_{36}(\theta) \end{bmatrix}. \tag{11}$$

Once the angular co-ordinates of nodes ① and ② for the arch element, θ_1 and θ_2, are given, one may obtain the values of matrix $[B]$ and its inverse $[B]^{-1}$ from Eq. (8). To insert the values of $[H]$ and $[B]^{-1}$ into Eq. (11) will determine the values of the shape function matrix $[N(\theta)]$. It is evident that the implicit shape functions given by Eq. (11) are much simpler than the explicit "exact" shape functions given in Tables 1–3 of Ref. [6], particularly for the computer programming. Based on the numerical example in Ref. [6], the 18 curves for the shape functions N_{mn} ($m = 1-3$; $n = 1-6$) were obtained from Eq. (11) and compared with the corresponding ones obtained from the explicit "exact" shape functions given in Tables 1–3 of Ref. [6] and excellent agreements were achieved [11].

In theory, the finite element method is an "approximate" method, thus the "exact" shape functions reported in Ref. [6] only mean that they enable the behavior of the arch to be calculated exactly for any mesh density (i.e., any number of arch elements) and they are also called the "natural" shape functions [7,8].

Table 1
The lowest five natural frequencies of a simply-supported arch, $\omega_i (i = 1-5)$ (rad/s), with rotary inertia neglected

Mode no. i	Exact solutions [7]	Present paper				
		By SB elements		By CB elements		
		20 elements	40 elements	2 elements	4 elements	6 elements
1	0.349	0.565	0.564	0.349	0.349	0.349
2	1.571	1.952	1.952	1.572	1.572	1.572
3	3.612	4.228	4.226	3.725	3.615	3.613
4	6.470	7.230	7.230	8.212	6.474	6.474
5	10.144	11.161	11.156	14.307	10.274	10.162

3. Stiffness matrix for arch element

From Ref. [1] one has the following force–displacement relations:

$$F_x = F'_\theta, \tag{12a}$$

$$F_\theta = \frac{EA}{R}(u'_\theta - u_x) - \frac{M_y}{R}, \tag{12b}$$

$$M_y = \frac{EI_y}{R^2}(u''_x + u_x), \tag{12c}$$

where the primes denote the derivatives with respect to the angular co-ordinate θ. From Eqs. (1) and (12) and the following relationship for the equilibrium of nodal forces

$$\{ F_{x1} \quad F_{\theta 1} \quad M_{y1} \} = -\{ F_{x2} \quad F_{\theta 2} \quad M_{y2} \}, \tag{13}$$

one obtains

$$\{F\} = [D]\,\{G\}, \tag{14}$$

where

$$\{F\} = \{ F_{x1} \quad F_{\theta 1} \quad M_{y1} \quad F_{x2} \quad F_{\theta 2} \quad M_{y2} \}, \tag{15}$$

$$[D] = \frac{EI_y}{R^2}\left[\begin{array}{ccc|ccc} 0 & 0 & 0 & -\frac{2}{R}\sin\theta_1 & 0 & -\frac{2}{R}\cos\theta_1 \\ 0 & 0 & 0 & \frac{2}{R}\cos\theta_1 & 0 & -\frac{2}{R}\sin\theta_1 \\ -1 & 0 & 0 & -2\cos\theta_1 & 0 & 2\sin\theta_1 \\ \hline 0 & 0 & 0 & \frac{2}{R}\sin\theta_2 & 0 & \frac{2}{R}\cos\theta_2 \\ 0 & 0 & 0 & -\frac{2}{R}\cos\theta_2 & 0 & \frac{2}{R}\sin\theta_2 \\ 1 & 0 & 0 & 2\cos\theta_2 & 0 & -2\sin\theta_2 \end{array}\right]. \tag{16}$$

Introducing the values of $[G]$ defined by Eq. (9) into Eq. (14) leads to

$$\{F\} = [D]\,[\mathrm{B}]^{-1} \quad \{\delta\} = [K]\{\delta\}, \tag{17}$$

where $[K]$ is the element stiffness matrix of the arch element and is given by

$$[K] = [D]\,[B]^{-1}. \tag{18}$$

4. Mass matrix for arch element

The kinetic energy of the arch element is given by

$$T = \tfrac{1}{2}\int_{\theta_1}^{\theta_2} \left[\rho A(\dot{u}_x^2 + \dot{u}_\theta^2) + \rho I_y \dot{\psi}_y^2\right] R\,\mathrm{d}\theta, \tag{19}$$

where the dots denote the derivatives with respect to time t, ρ is the mass density of the arch material and I_y is the moment of inertia of the cross-sectional area defined by Eq. (3). It is noted that the third term on the right-hand side of Eq. (19), $\rho I_y \dot{\psi}_y^2$, represents the rotary inertia, which is not considered in Refs. [7,8].

For harmonic free vibrations, one has

$$\{u\} = \{\bar{u}\}\,\mathrm{e}^{\mathrm{i}\omega t}, \tag{20}$$

where $\{\bar{u}\}$ is the amplitude of $\{u\}$, ω is the natural frequency of the arch, t is time and $\mathrm{i} = \sqrt{-1}$.

The substitution of Eqs. (4) and (20) into Eq. (19) yields

$$T = \tfrac{1}{2}\omega^2 \{\delta\}^{\mathrm{T}}[M]\{\delta\}, \tag{21}$$

where $[M]$ is the consistent mass matrix of the arch element given by

$$[M] = \rho R([B]^{-1})^{\mathrm{T}} \left(\int_{\theta_1}^{\theta_2} [H]^{\mathrm{T}}[\Lambda][H]\,\mathrm{d}\theta\right) [B]^{-1}, \tag{22}$$

with

$$[\Lambda] = \begin{bmatrix} A & 0 & 0 \\ 0 & A & 0 \\ 0 & 0 & I_y \end{bmatrix}. \tag{23}$$

To determine the consistent mass matrix of an arch element, $[M]$, using Eq. (22), it is only required to calculate the following integration:

$$[\bar{H}] = \int_{\theta_1}^{\theta_2} [H]^{\mathrm{T}}[\Lambda][H]\,\mathrm{d}\theta, \tag{24}$$

and all the other numerical calculations are performed by computer. Because $[\bar{H}]$ is a 6×6 symmetrical square matrix, one requires only to calculate the 21 coefficients of the matrix. This is also much simpler than the 108 constants for the 18 shape functions shown in Tables 1–3 of Ref. [6]. For the explicit form of the matrix $[\bar{H}]$, one may refer to Ref. [11].

5. External loading vector due to a moving load

For an arch subjected to a moving load with magnitude P along the circumferential direction, all nodal forces of the whole arch are equal to zero except those of the arch element on which the moving load P applies. The non-zero elemental nodal force vector is given by (see Fig. 2)

$$\{F\} = \left[\{a_x(\theta)\} \quad \{a_z(\theta)\} \right] \begin{Bmatrix} f_x \\ f_z \end{Bmatrix}, \tag{25}$$

where

$$\{F\} = \left\{ F_{x1} \quad F_{\theta 1} \quad M_{y1} \quad F_{x2} \quad F_{\theta 2} \quad M_{y2} \right\}, \tag{26}$$

$$\{a_x(\theta)\} = \left\{ N_{11}(\theta) \quad N_{12}(\theta) \quad \cdots \quad N_{16}(\theta) \right\}, \tag{27}$$

$$\{a_z(\theta)\} = \left\{ N_{21}(\theta) \quad N_{22}(\theta) \quad \cdots \quad N_{26}(\theta) \right\}. \tag{28}$$

In Eqs. (27) and (28), $N_{ij}(\theta), i = 1, 2$ and $j = 1-6$, represent the shape functions defined by Eq. (11), while in Eq. (25), f_x and f_z represent the radial and tangential external force components at the application point of the moving load, respectively, and are given by

$$f_x = P \cos \phi - F_c, \tag{29}$$

$$f_z = -F_f - P \sin \phi, \tag{30}$$

where F_c and F_f are the centrifugal force and the frictional force, respectively. If the mass of the moving load is m_P, the moving speed in the tangential direction is V_P and the radius of curvature of the arch is R, then the value of the centrifugal force is determined by

$$F_c = m_P V_P^2 / R. \tag{31}$$

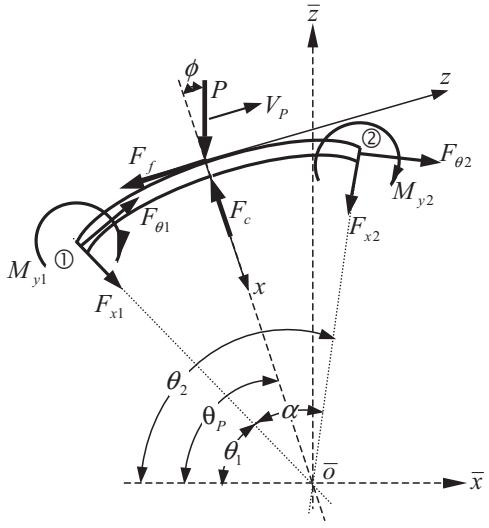

Fig. 2. The nodal forces, F_{x1}, $F_{\theta 1}$, M_{y1}, F_{x2}, $F_{\theta 2}$ and M_{y2}, for the arch element on which the moving load P applies.

Similarly, if the frictional coefficient between the moving load and the arch is μ, then the frictional force is defined by

$$F_f = \mu f_x. \tag{32}$$

In the above equations, ϕ is the angle between the moving load P and the local radial x-axis. From Fig. 2 one sees that ϕ is dependent upon the circular co-ordinate θ_P, defining the position of the moving load P, i.e.,

$$\phi = \frac{\pi}{2} - \theta_P. \tag{33}$$

It is noted that the frictional force $F_f = \mu P \cos\phi$ and the tangential component of the moving load, $P \sin\phi$, are in the same direction if $\theta_P < \pi/2$, and in the opposite direction if $\theta_P > \pi/2$.

If the title problem is solved with the conventional finite straight-beam elements, then the external nodal force vector given by Eq. (25) must be replaced by (see Fig. 3)

$$\{F\} = \begin{bmatrix} \{a_x(\xi)\} & \{a_z(\xi)\} \end{bmatrix} \begin{Bmatrix} f_x \\ f_z \end{Bmatrix}, \tag{34}$$

where

$$\{F\} = \begin{Bmatrix} F_1 & F_2 & \cdots & F_6 \end{Bmatrix}, \tag{35}$$

$$\{a_x(\xi)\} = \begin{Bmatrix} a_{x1} & a_{x2} & \cdots & a_{x6} \end{Bmatrix}, \tag{36}$$

$$\{a_z(\xi)\} = \begin{Bmatrix} a_{z1} & a_{z2} & \cdots & a_{z6} \end{Bmatrix}, \tag{37}$$

$$\xi = \frac{z}{\ell}, \tag{38}$$

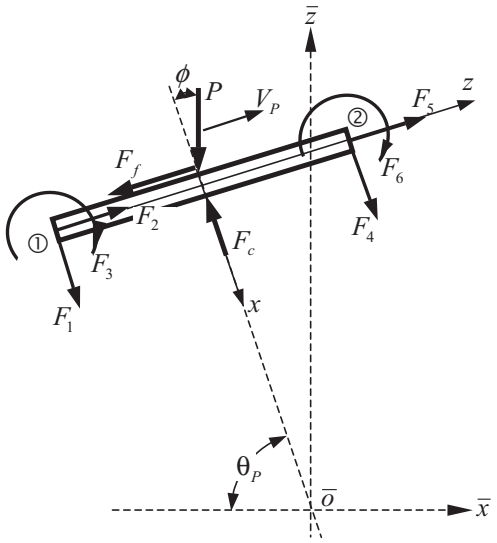

Fig. 3. The nodal forces $F_i (i = 1-6)$ for the straight-beam element on which the moving load P applies.

$$\begin{cases} a_{x1} = 1 - 3\xi^2 + 2\xi^3 \\ a_{x2} = 0 \\ a_{x3} = \left(\xi - 2\xi^2 + \xi^3\right)\ell \\ a_{x4} = 3\xi^2 - 2\xi^3 \\ a_{x5} = 0 \\ a_{x6} = \left(-\xi^2 + \xi^3\right)\ell \end{cases} \qquad \begin{cases} a_{z1} = 0 \\ a_{z2} = 1 - \xi \\ a_{z3} = 0 \\ a_{z4} = 0 \\ a_{z5} = \xi \\ a_{z6} = 0 \end{cases} . \tag{39a, b}$$

In Eq. (38), z is the local co-ordinate for the instantaneous position of the moving load P and ℓ is the length of the straight-beam element shown in Fig. 3. In Eqs. (39a) and (39b), a_{xi} and a_{zi}, $i = 1-6$, are the shape functions for the straight-beam element [12]. For a horizontal straight beam, $\theta_P \equiv \pi/2$, $\phi \equiv 0$ and $R = \infty$, thus from Eqs. (29)–(32) one obtains

$$f_x = P, \tag{40}$$

$$f_z = \mu P. \tag{41}$$

6. Displacements from curved-beam and straight-beam elements

The relationship between the nodal displacements for the curved-beam (CB) element, u_{x1}, $u_{\theta 1}$, ψ_{y1},… and ψ_{y2}, and those for the straight-beam (SB) element, $\bar{u}_1$, $\bar{u}_2$, $\bar{u}_3$,… and $\bar{u}_6$, are shown in Fig. 4, where the CB (arch) element is represented by the solid lines and the SB element by the dashed lines. Since all the stiffness and mass matrices of the SB elements must be transformed to the ones with respect to the global co-ordinate system, $\overline{xyz}$, and then are assembled to establish the overall stiffness and mass matrices of the whole structure, the computer outputs for either the modal displacements obtained from the free vibration analysis or the actual displacements obtained from the forced vibration analysis are with respect to the global co-ordinate systems, $\overline{xyz}$, when the problem is solved with the SB elements. This is the reason why the nodal displacements with respect to the global ($\overline{xyz}$) co-ordinate system, $\bar{u}_i (i = 1-6)$, instead of those with respect to the local (xyz) co-ordinate system, $u_i (i = 1-6)$, were shown in Fig. 4. It is evident that all the directions of the nodal displacements for the CB element are different from those for the SB element except the rotational angles

$$\bar{u}_3 = \psi_{y1}, \quad \bar{u}_6 = \psi_{y2}. \tag{42a, b}$$

Therefore, the following expressions should be used to transform the displacement components obtained from the CB elements, u_{xi} and $u_{\theta i} (i = 1, 2)$, into the vertical ones (in the $\bar{z}$-direction), $d_{\bar{z}i} (i = 1, 2)$, if comparisons between the arch elements and the SB elements are based on the vertical displacements:

$$d_{\bar{z}1} = -u_{x1} \cos\beta + u_{\theta 1} \sin\beta \ \text{(for node ①)}, \tag{43a}$$

$$d_{\bar{z}2} = -u_{x2} \cos\gamma - u_{\theta 2} \sin\gamma \ \text{(for node ②)}, \tag{43b}$$

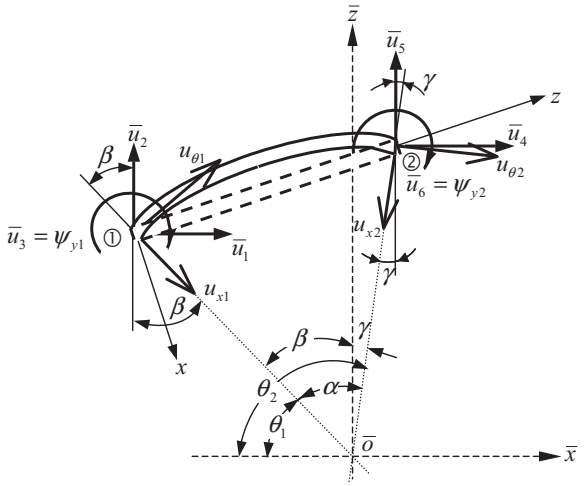

Fig. 4. The relationship between the nodal displacements for the curved-beam (arch) element (u_{x1}, $u_{\theta 1}$, $\psi_{y1}, \ldots, \psi_{y2}$) and the straight-beam element ($\bar{u}_1$, $\bar{u}_2$, $\bar{u}_3, \ldots, \bar{u}_6$).

where β and γ are the angles between the radii passing through nodes ① and ② and the vertical $\bar{z}$-axis, respectively, as shown in Fig. 4. The positive values of $d_{\bar{z}1}$ and $d_{\bar{z}2}$ indicate the vertical displacements in the upward ($+\bar{z}$) direction.

Similarly, if the comparisons are based on the radial displacements, then one should use the following relations to transform the nodal displacements of the SB element, $\bar{u}_i (i = 1, 2, 4, 5)$, into the radial ones:

$$d_{r1} = \bar{u}_1 \sin\beta - \bar{u}_2 \cos\beta \ \text{(for node ①)}, \tag{44a}$$

$$d_{r2} = \bar{u}_4 \sin\gamma - \bar{u}_5 \cos\gamma \ \text{(for node 2)}. \tag{44b}$$

The positive values of d_{r1} and d_{r2} indicate the radial displacements pointing to the curvature center $\bar{o}$ of the arch (i.e., to the $+u_{xi}$ direction, $i = 1, 2$).

In this paper, all the curves were plotted based on the vertical nodal displacements, thus Eqs. (43a) and (43b) were used for the transformations.

7. Numerical results and discussions

To confirm the reliability of the presented theory, the natural frequencies and the forced vibration responses obtained from the arch elements are compared with the existing literature and those from the conventional finite straight-beam elements, respectively. After that, the dynamic behaviors of a 120° circular arch and a hybrid (curved) beam due to a moving load are investigated using the Newmark direct integration method [13]. Unless particularly stated, all the numerical results presented in this paper were obtained based on the arch elements with the effect of rotary inertia considered. In addition, both the centrifugal force and the frictional force (with coefficient $\mu = 0.2$) were also taken into account.

7.1. Validation of natural frequencies

Information regarding the free vibration analysis of arches is rare. Refs. [7–9] are the literature that has been found to be most concerned. The dimensions and the material constants for the present example are [7]: radius of curvature $R = 30$ in, radial thickness of rib $a = 1.289 \times 10^{-2}$ in, axial width of rib $b = 1.008$ in, cross-sectional area $A = 0.013$ in^2, subtended angle of the complete arch $\bar{\alpha} = 1$ rad $= 57.3^\circ$, total (arc) length $\ell = R\bar{\alpha} = 30$ in, Young's modulus $E = 10^7$ lb/in^2, mass density of arch material $\rho = 0.1$ lb/in^3.

The lowest five natural frequencies $\omega_i (i = 1-5)$ (rad/s) of the arch are shown in Table 1 for the simply-supported conditions (with radial displacements $u_{xL} = u_{xR} = 0$**).** Where the right subscripts L and R refer to the *left* end and *right* end of the circular arch, respectively. The natural frequencies listed in column 2 of Table 1 are the exact solutions calculated from the frequency equation list in the appendix of Ref. [7] and those listed in columns 3–7 are the finite element solutions of this paper. Among the latter, those in columns 3 and 4 are obtained using the SB elements and those in columns 5–7 using the CB elements. It is seen that all the natural frequencies obtained from the CB elements rapidly converge to the corresponding exact ones when the total number of elements increases from $n = 2$ to 6, but this in not true for the SB elements even if $n = 40$. From Table 1 one also sees that the natural frequencies obtained from the finite element methods (either based on SB or CB elements) are larger than the exact solutions and converge monotonically to the exact ones from above. This trend of finite element solutions agrees with that of Ref. [7].

For a uniform arch, both the element stiffness matrix and element mass matrix are invariant if the subtended angle of the arch element, α, is a constant as one may see from the output of the computer program. In addition, because the formulations for the arches are based on the polar co-ordinate system, transformation of each element property matrix (from local co-ordinate system into global one) is not required before assembling. This is another advantage that the CB elements are superior to the SB elements for the dynamic analysis of arches.

7.2. Validation of forced vibration responses

Since the information regarding the forced vibration responses of an arch due to the moving load(s) is not obtainable, the indirect comparing technique was used to confirm the reliability of the presented theory. Fig. 5 shows a circular arch with constant span $L = 10$ m, constant cross-section 0.8 m $\times$ 1.5 m and variable radius of curvature R. The material constants for the arch are: Young's modulus $E = 12 \times 10^{10}$ N/m^2 and mass density $\rho = 7.2 \times 10^3$ kg/m^3. It is evident that the circular arch will become a "*straight beam*" when $R \to \infty$. In Fig. 6, the uppermost curve (—•—) indicates the relationship between the maximum vertical central displacements ($|\delta_{58}|_{\max}$) and the tangential moving speed (V_P) for the above-mentioned "*straight beam*" subjected to a moving load with constant magnitude $P = 50,000$ N, while the lowermost curve (- - - - -) indicates that for the circular arch of $R = 20$ m subjected to the same moving load. It is noted that the centrifugal forces for the circular arches are neglected in Fig. 6, because there exists no centrifugal force for the "*straight beam*". From Fig. 6 one sees that the curve for the circular arch gradually converges to the uppermost curve when the radius of curvature gradually increases to infinity (i.e., $R \to \infty$), besides, the maximum vertical central displacement of the "*straight beam*" is greater than

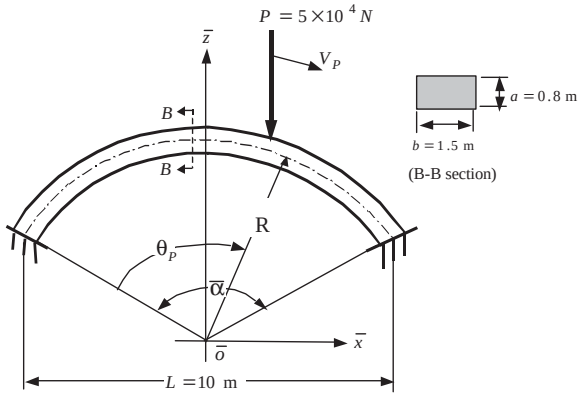

Fig. 5. A clamped–clamped circular arch with constant span $L = 10$ m, constant cross-section 0.8 m × 1.5 m and variable radius of curvature R, subjected to a moving load with constant magnitude $P = 50,000$ N and tangential speed V_P.

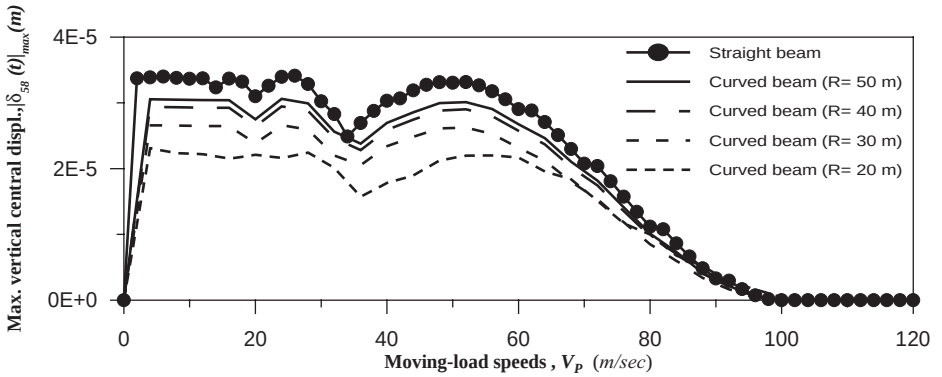

Fig. 6. Influence of radius of curvature (R) and tangential moving speed (V_P) on the maximum vertical central displacements ($|\delta_{58}(t)|_{\max}$) of the arch shown in Fig. 5 subjected to a moving load with constant magnitude $P = 50,000$ N.

the corresponding one of the associated circular arch. It is believed that the last reasonable results may confirm the availability of the presented approach.

7.3. Dynamic analysis of a clamped–clamped arch due to a moving load

For the clamped–clamped circular arch, as shown in Fig. 5, if the average radius of curvature is $R = 20$ m and the subtended angle is $\bar{\alpha} = 120^\circ$(with corresponding span $L = 34.64$ m), then the lowest five natural frequencies and the corresponding mode shapes are shown in Table 2 and Figs. 13(a)–(e), respectively. From Table 2 one sees that the lowest five natural frequencies for the case of considering the effect of rotatory inertia (R.I.) are smaller than the corresponding ones for the case of neglecting the effect of R.I., but the divergence between them is very small for the present example. When the 120° circular arch is subjected to a moving load with magnitude $P = 50,000$ N and moving speed V_P, then its dynamic responses are shown in Figs. 7(a)–(c): Fig. 7(a)

Table 2
The lowest five natural frequencies of the 120° circular arch (cf., Fig. 5)

Mode nos. i	Natural frequencies, ω_i (rad/s)			
	Clamped–clamped		Hinged–hinged	
	Consider R.I.	Neglect R.I.	Consider R.I.	Neglect R.I.
1	27.892	27.905	16.316	16.322
2	54.993	55.055	41.069	41.110
3	100.710	100.941	79.357	79.524
4	143.866	144.285	124.036	124.430
5	198.849	199.141	184.173	185.098

shows the time histories for the vertical displacements of nodes 11 and 21, $\delta_{28}(t)$ and $\delta_{58}(t)$. It is noted that the whole arch is subdivided into 40 curved-beam elements bound by 41 nodes, each node has three degrees of freedom (d.o.f.), and the right subscript i for $\delta_i(t)$ denotes the ith d.o.f. for the whole arch (excluding the constrained d.o.f.). The effects of the centrifugal force, F_c, and frictional force, F_f (with frictional coefficient μ), on the maximum vertical central displacements of the arch, $|\delta_{58}(t)|_{\max}$, are shown in Figs. 7(b) and (c), respectively.

In Fig. 7(a), the solid line (——) represents the time history for node 11 (located at $\frac{1}{4}$ of the arch length) and the dashed line (– – –) represents that for node 21 (located at $\frac{1}{2}$ of the arch length). It is seen that the maximum vertical displacement of node 11, $|\delta_{28}(t)|_{\max}$, is much greater than that of node 21, $|\delta_{58}(t)|_{\max}$. This is a correct result, because node 11 is near the "crest" of the first and second mode shapes, while node 21 (at middle of the arch) is near the "node" of the first and second mode shapes as one may see from Figs. 13(a) and (b). Besides, the vertical displacement increases rapidly when the load moves near the specified node (11 or 21) and decreases rapidly when the load moves away from the specified node.

In Fig. 7(b), the solid line (——) denotes the relationship between the maximum vertical central displacements of the circular arch, $|\delta_{58}(t)|_{\max}$, and the moving speeds V_P for the case of considering the centrifugal force, F_c, while the dashed line (– – –) denotes that for the case of neglecting the centrifugal force. It is evident that the maximum vertical central displacements of the circular arch, $|\delta_{58}(t)|_{\max}$, by considering the centrifugal force are always less than the corresponding ones by neglecting the centrifugal force, furthermore, the higher the moving speed V_P the larger the divergence between them as one may expect. The solid line meets the abscissa of the figure when $V_P \geqslant 14.14$ m/s, because, in such a situation, the centrifugal force greater than the radial force component due to the moving load P.

In Fig. 7(c), the solid line (——) denotes the relationship between the maximum vertical central displacements of the circular arch, $|\delta_{58}(t)|_{\max}$, and the moving speeds V_P for the case of considering the frictional force, F_f (with frictional coefficient $\mu = 0.2$), while the dashed line (– –) denotes that for the case of neglecting the frictional force (with $\mu = 0$). It is seen that the frictional force has a slight effect of reducing the maximum vertical central displacements of the circular arch.

In addition to the maximum deflections, the dynamic magnification factor defined by

$$D_i = |\delta_i(t)|_{\max}/\delta_{st\ \mathrm{i}} \tag{45}$$

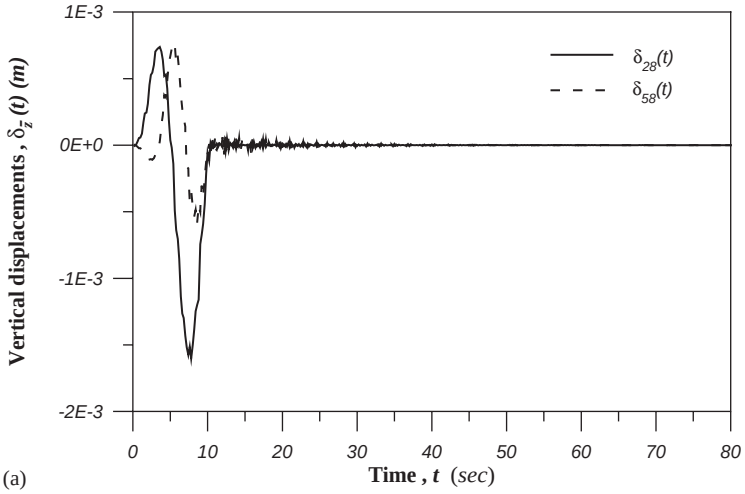

(a)

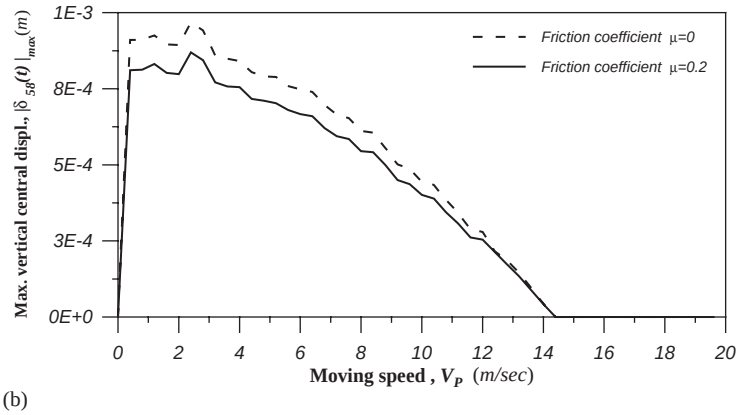

(b)

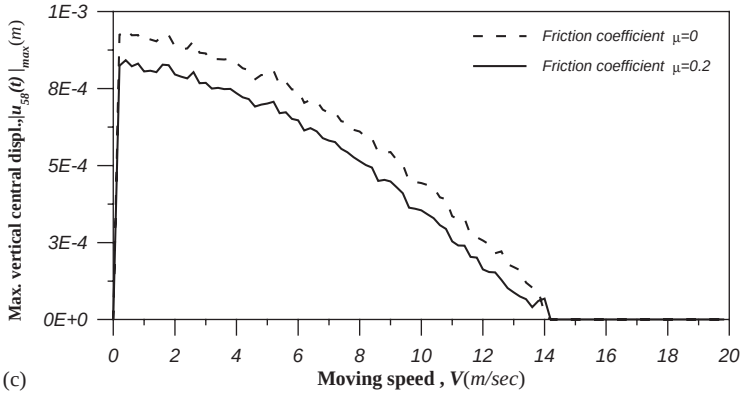

(c)

Fig. 7. Dynamic responses of the "clamped–clamped" 120° circular arch due to a moving load with $P = 50,000$ N: (a) time histories for the vertical displacements of nodes 11 and 21, $\delta_{28}(t)$ and $\delta_{58}(t)$ with $V_P = 4$ m/s; (b) influence of centrifugal force (F_c) and moving speed (V_P) on the maximum vertical central displacements of the arch, $|\delta_{58}(t)|_{\max}$; (c) influence of frictional force, F_f (with frictional coefficient μ) and moving speed (V_P) on $|\delta_{58}(t)|_{\max}$. The vertical static deflection at the midpoint of the beam is $\delta_{st\ 58} = 0.18357 \times 10^{-4}$ m.

is also an important parameter for the engineers, thus, in Figs. 7, 8 and 10–12, the values of δ_{sti} were shown in the captions. For example, from the caption of Fig. 7 one sees that $\delta_{st\ 58} = 0.18357 \times 10^{-4}$ m and the ordinates of Figs. 7(b) and (c) will denote the associated magnification factors if all the values of $|\delta_{58}(t)|_{\max}$ are divided by $\delta_{st\ 58}$. In Eq. (45), $|\delta_i(t)|_{\max}$ denotes the maximum nodal displacement in the direction of ith degree of freedom and $\delta_{st\ i}$ denotes the corresponding "static" deflection due to the "static load" with magnitude being equal to the amplitude of the dynamic load.

7.4. Dynamic analysis of a hinged–hinged arch due to a moving load

If all the particulars for the circular arch are the same as the last example but the supporting conditions are hinged–hinged (instead of clamped–clamped), then the lowest five natural frequencies and the corresponding mode shapes are shown in Table 2 and Figs. 14(a)–(e), respectively, while the forced vibration responses due to a moving load (with $P = 50,000$ N and speed V_P) are shown in Figs. 8(a)–(c). From Table 2 one sees that the lowest five natural frequencies of the hinged–hinged arch are much lower than the corresponding ones of the clamped–clamped arch, but the configurations of the lowest five mode shapes for the hinged–hinged arch are similar to those for the clamped–clamped one. For example, node 11 is near the "crest" of the first and second mode shapes and node 21 (at the middle of the arch) is near the "node" of first and second mode shapes as one may see from Figs. 14(a) and (b). For this reason, the trends for the time histories of nodes 11 and 21 (see Fig. 8(a)), the influence of centrifugal force (F_c) on the maximum vertical central displacements (see Fig. 8(b)) and the effect of the frictional force with coefficient μ (see Fig. 8(c)) for the hinged–hinged arch are similar to the corresponding ones for the clamped–clamped arch as shown in Figs. 7(a)–(c). However, the maximum vertical (central) displacements of the hinged-hinged arch are much greater than the corresponding ones of the clamped–clamped arch. This is reasonable, because the flexural rigidity of the hinged–hinged arch is much smaller than that of the clamped–clamped arch. Of course, this is also the reason why the lowest five natural frequencies of the hinged–hinged arch are much smaller than those of the clamped–clamped arch as shown in Table 2.

7.5. Dynamic responses of a hybrid (curved) beam due to a moving load

The hybrid (curved) beam studied here is shown in Fig. 9. It is composed of a circular-arch segment with radius of curvature $R = 20$ m and subtended angle $\bar{\alpha} = 120^\circ$ and two identical straight-beam segments. Both the arch segment and the two straight-beam segments have the same cross-sections: 0.8 m × 1.5 m. The two ends of the hybrid beam are clamped, but the conjunctions between the arch segment and the two straight- beam segments, points P and Q, are hinged. Since the total number of finite elements for each straight-beam segment is 10 and that for the circular arch is 20, the total number of finite elements, 40, and that of nodes, 41, for the whole hybrid beam are exactly the same as those for the 120° circular arch studied in the last two subsections. The dynamic responses of the hybrid beam due to a moving load with magnitude $P = 50,000$ N and tangential speed $V_P = 4$ m/s are shown Figs. 10(a)–(c).

Fig 10(a) shows the time histories of the vertical displacements of nodes 16 and 21, $\delta_{41}(t)$ and $\delta_{56}(t)$, obtained from the conventional finite elements with all parts (either the two identical

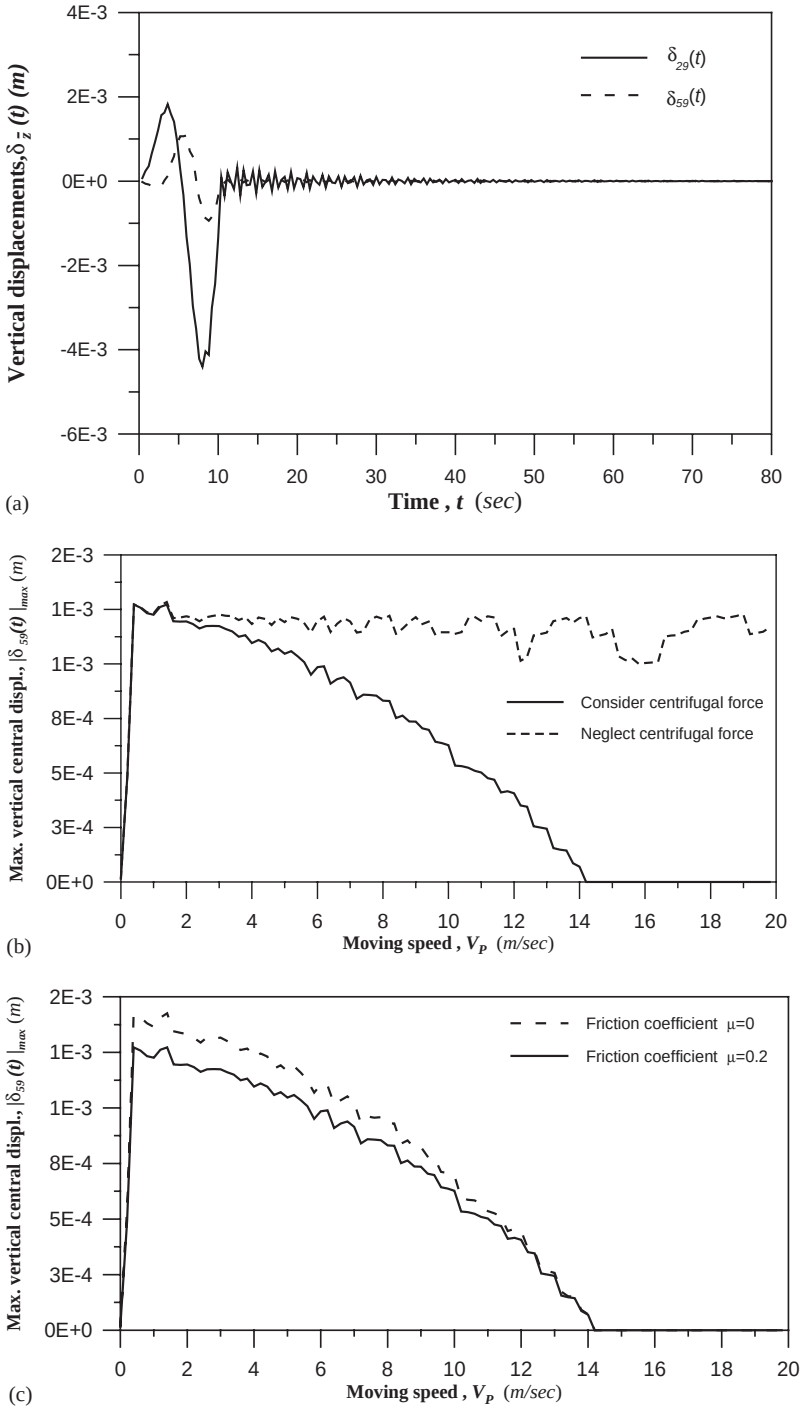

Fig. 8. Dynamic responses of the "hinged–hinged" 120° circular arch due to a moving load with $P = 50,000$ N: (a) time histories for the vertical displacements of nodes 11 and 21, $\delta_{29}(t)$ and $\delta_{59}(t)$ with $V_P = 4$ m/s; (b) influence of centrifugal force (F_c) and moving speed (V_P) on the maximum vertical central displacements of the arch, $|\delta_{59}(t)|_{\max}$; (c) influence of frictional force (with frictional coefficient μ) and moving speed (V_P) on $|\delta_{59}(t)|_{\max}$. The vertical static deflection at the midpoint of the beam is $\delta_{st\ 59} = 0.85578 \times 10^{-4}$ m.

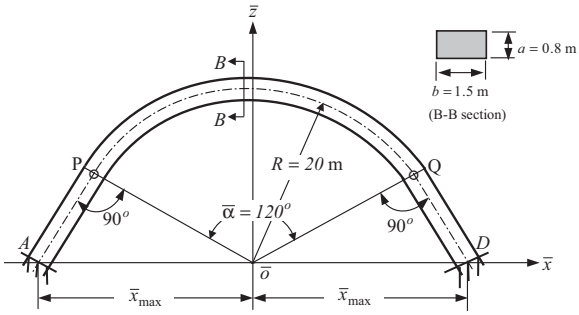

Fig. 9. A clamped–clamped hybrid (curved) beam composed of a circular-arch segment (with radius of curvature $R = 20$ m and subtended angle $\bar{\alpha} = 120°$) and two identical straight-beam segments. The dimensions for each cross-section are: 0.8 m × 1.5 m. Conjunctions, P and Q, are hinged.

straight-beam segments or the circular-arch segment) being modelled by the straight-beam elements. For this reason, the curves obtained from the conventional straight-beam elements are called the S–S curves hereafter. It is noted that the positions of nodes 16 and 21 on the hybrid beam shown in Fig. 9 are corresponding to those of nodes 11 and 21 on the 120° circular arch shown in Fig. 5. The moving speed for either Figs. (7a), 8(a) or 10(a) is $V_p = 4$ m/s.

In Figs. 10(b) and (c), the S–C curves denote the dynamic responses of the hybrid beam obtained from a combination of the straight-beam elements (to model the two identical straight-beam segments) and the curved-beam (arch) elements (to model the 120° circular-arch segment). It is seen that the maximum vertical central displacements for the hybrid beam, $|\delta_{56}(t)|_{\max}$, associated with the S–C curves are smaller than the corresponding ones associated with the S–S curves. However, both the S–C curves and the S–S curves have the same trend. It is noted that, in the S–C method, all the property matrices for either the straight-beam elements or the curved-beam elements must be transformed into the ones associated with the common global co-ordinate system before they are assembled to establish the overall property matrices of the entire hybrid curved beam. Of course, transformation for the external force vectors given by Eqs. (25) and (34) is also required.

7.6. *Influence of rotatory inertia*

From Table 2 one sees that the influence of rotatory inertia (R.I.) on the lowest five natural frequencies is negligible for the arch studied in this paper. This is the reason why the influence of rotatory inertia (R.I.) on the dynamic responses is also negligible as one may see from Fig. 11. In Fig. 11, the ordinates denote the dynamic magnification factors of the vertical central displacements ($D_i = |\delta_i(t)|_{\max}/\delta_{sti}$) and the abscissas denote the moving-load speeds. Among the three figures, Fig. 11(a) is for the "clamped–clamped" 120° arch with static deflection $\delta_{st\ 58} = 0.18357 \times 10^{-4}$ m, Fig. 11(b) is for the "hinged–hinged" 120° arch with $\delta_{st\ 59} = 0.85578 \times 10^{-4}$ m, and Fig. 11(c) is for the hybrid beam with $\delta_{st\ 56} = 0.35445 \times 10^{-4}$ m.

From Figs. 11(a) and (b) one sees that the magnification factor of the midpoint for the "clamped–clamped" 120° arch, $D_{58} \approx 47.5$, is much greater than that for the same arch with "hinged–hinged" supports, $D_{59} \approx 14$. However, this does not mean that the maximum vertical

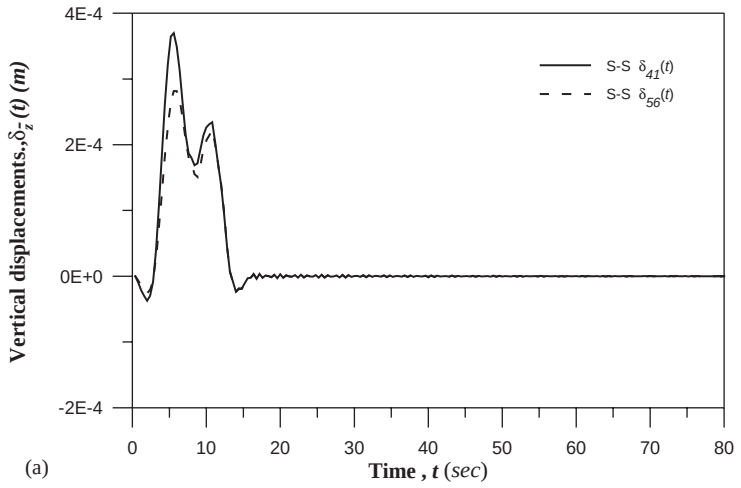

(a)

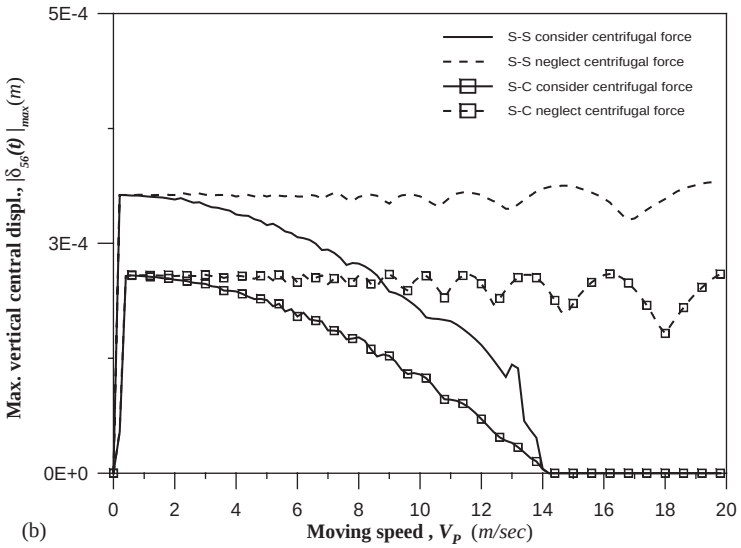

(b)

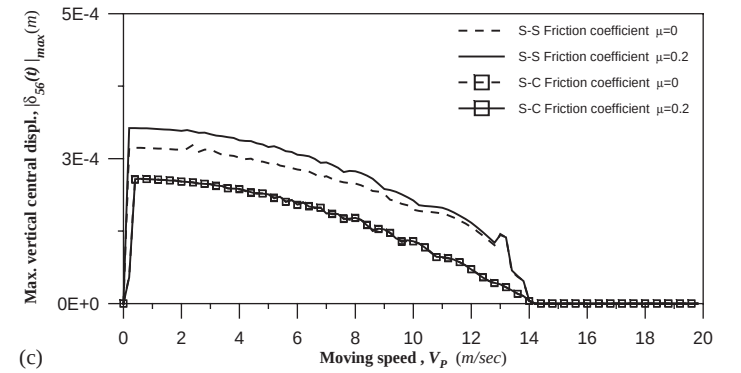

(c)

Fig. 10. Dynamic responses of the "hybrid beam" subjected to a moving load with $P = 50,000$ N: (a) time histories for the vertical displacements of nodes 16 and 21, $\delta_{41}(t)$ and $\delta_{56}(t)$ with $V_P = 4$ m/s; (b) influence of centrifugal force (F_c) and moving speed (V_P) on the maximum vertical central displacements of the beam, $|\delta_{56}(t)|_{\max}$; (c) influence of frictional force (with frictional coefficient μ) and moving speed (V_P) on $|\delta_{56}(t)|_{\max}$. The vertical static deflection at the midpoint of the beam is $\delta_{st\ 56} = 0.35445 \times 10^{-4}$ m.

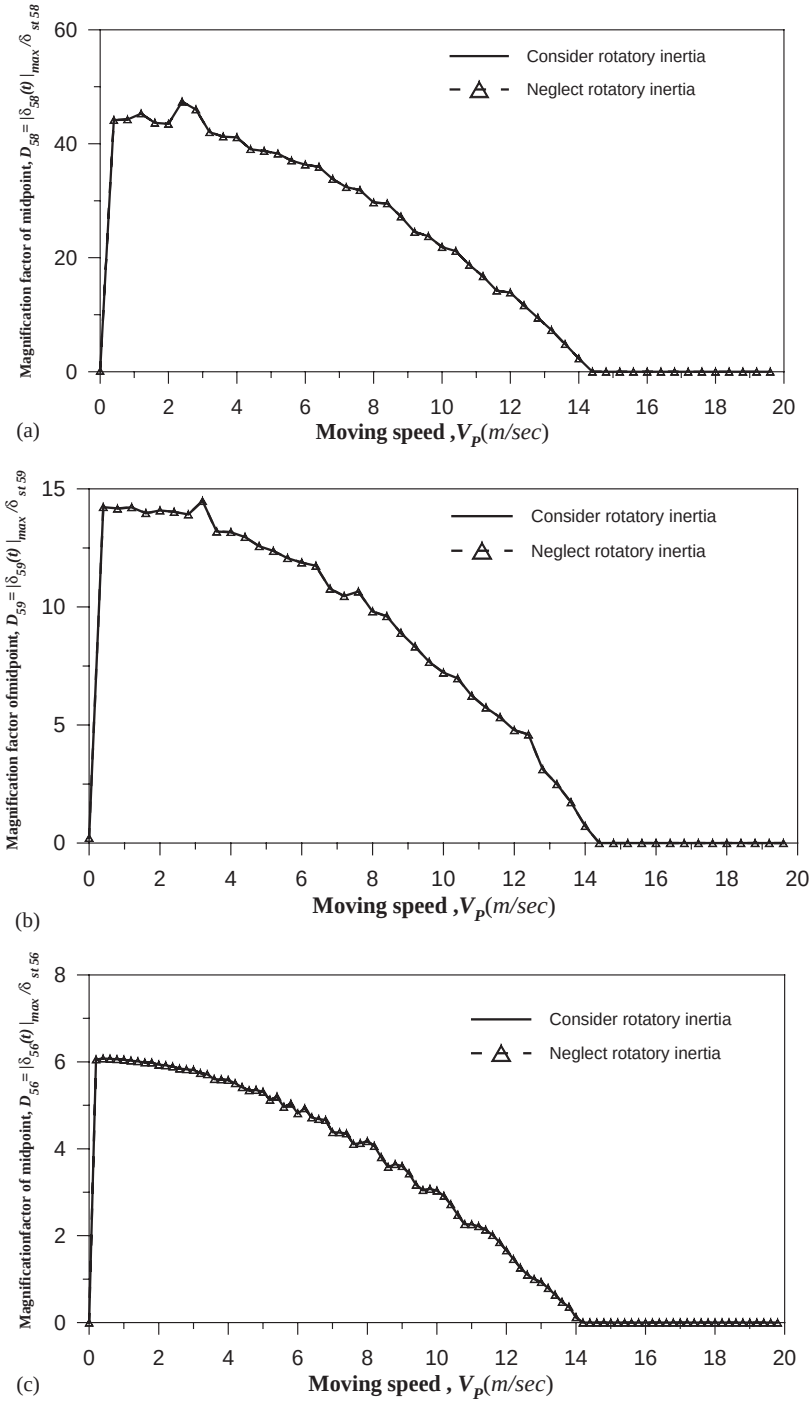

Fig. 11. Influence of rotatory inertia (R.I.) and moving speed (V_P) on the dynamic magnification factors of the vertical central displacements, $D_i = |\delta_i(t)|_{\max}/\delta_{st\ i}$: (a) for "clamped–clamped" 120° arch with $\delta_{st\ 58} = 0.18357 \times 10^{-4}$ m; (b) for "hinged–hinged" 120° arch with $\delta_{st\ 59} = 0.85578 \times 10^{-4}$ m, and (c) for hybrid beam with $\delta_{st\ 56} = 0.35445 \times 10^{-4}$ m.

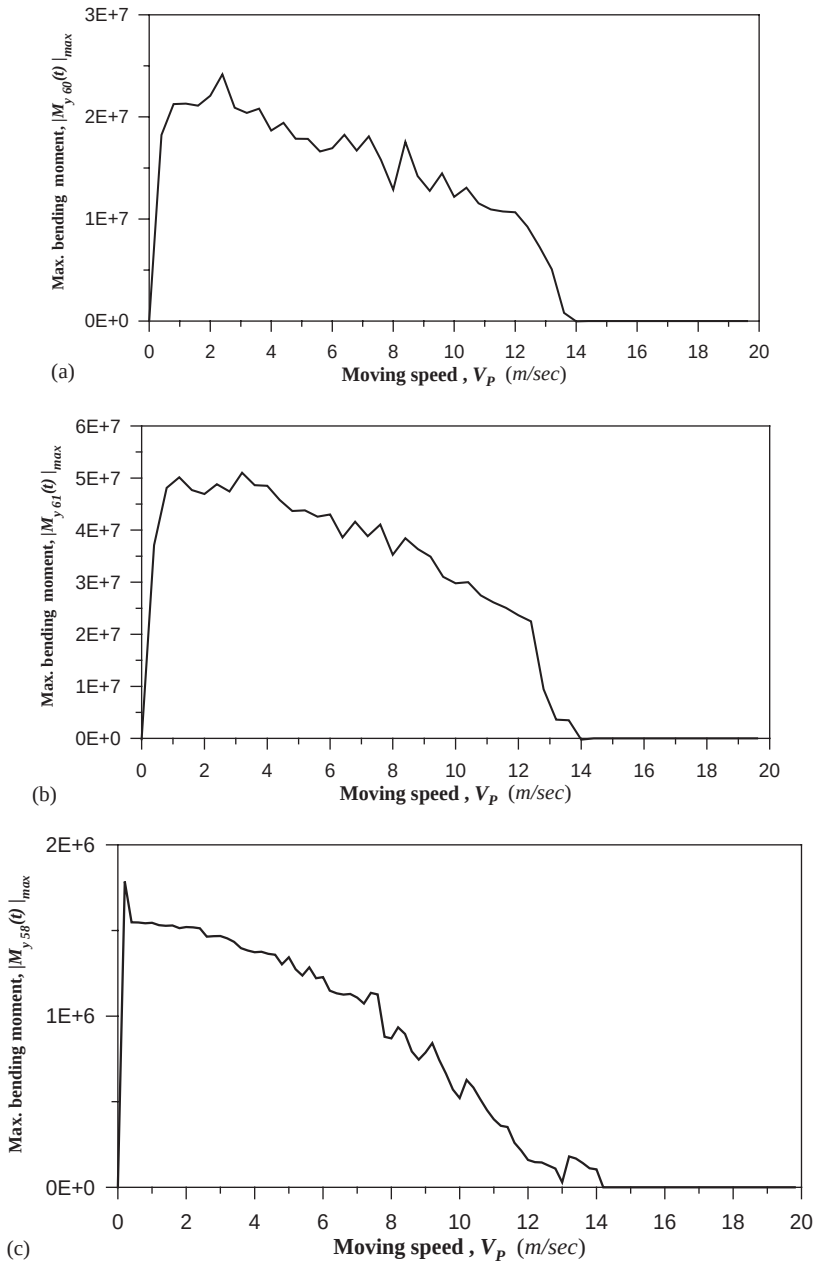

Fig. 12. Influence of moving-load speed (V_P) on the maximum bending moments about the y-axis at the midpoints of the beams, $|M_{y\,i}(t)|_{\max}$: (a) for "clamped–clamped" 120° arch, (b) for "hinged–hinged" 120° arch, and (c) for hybrid beam shown in Fig. 9.

central displacements of the 120° arch with "clamped–clamped" supports are much greater than the corresponding ones with "hinged–hinged" supports. The actual situation is reversed as one may see from the following statement. The "overall" maximum vertical central displacement of

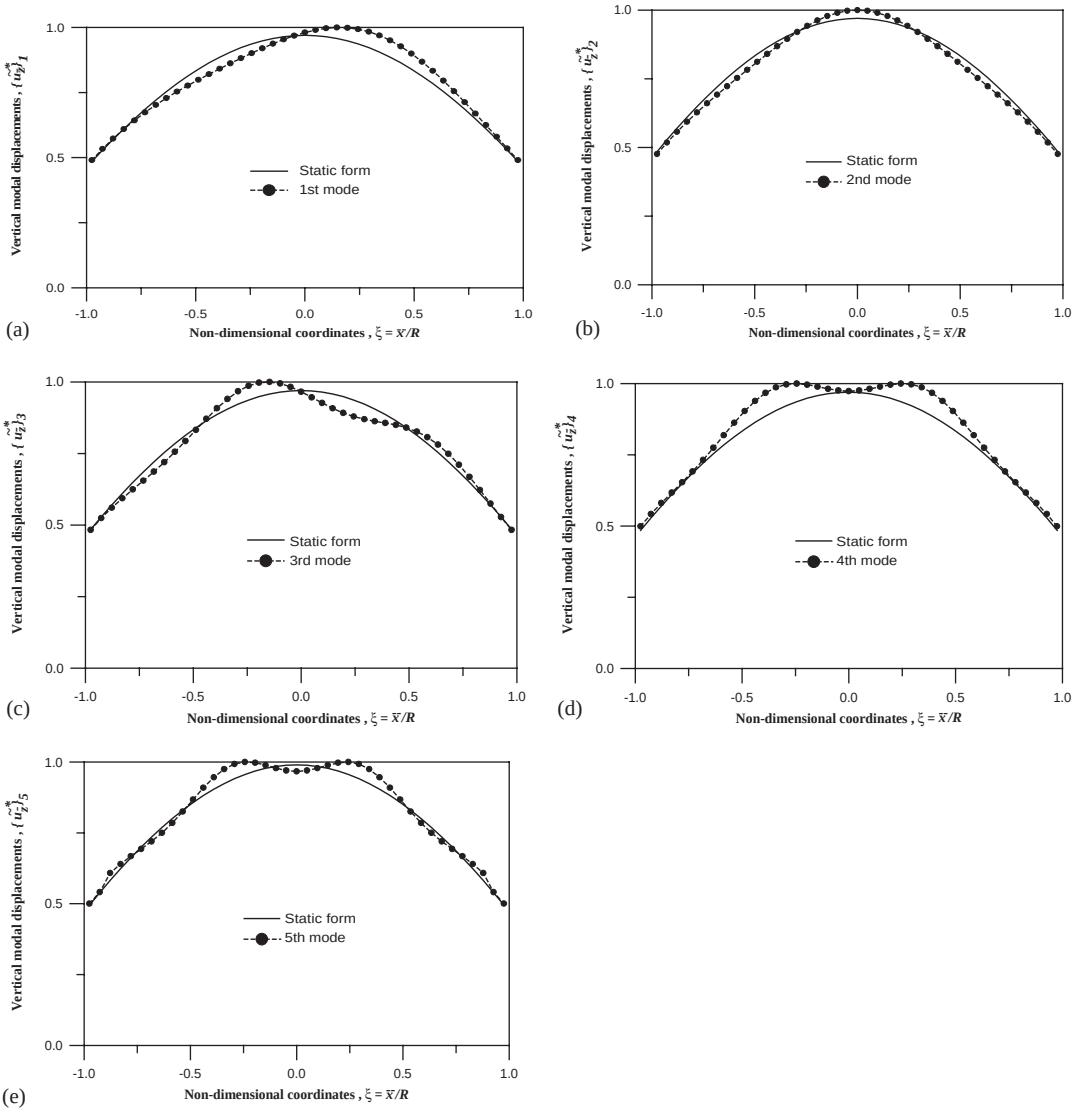

Fig. 13. The lowest five mode shapes of the *clamped–clamped* 120° circular arch (cf., Fig. 5).

the 120° arch with "clamped–clamped" supports is given by (see Fig. 11(a))

$$|\delta_{58}(t)|_{\max} = D_{58}\delta_{st58} \approx 47.5 \times 0.18357 \times 10^{-4} = 8.72 \times 10^{-4} \text{ m}, \tag{46a}$$

and that with "hinged–hinged" supports is given by (see Fig. 11(b))

$$|\delta_{59}(t)|_{\max} = D_{59}\delta_{st59} \approx 14 \times 0.85578 \times 10^{-4} = 11.98 \times 10^{-4} \text{ m}. \tag{46b}$$

From Eqs. (46a) and (46b), one sees that the "overall" maximum vertical central displacement of the 120° arch with "clamped–clamped" supports is about 72.8% of that with "hinged–hinged" supports. This is a reasonable result, because the flexural stiffness of the 120° arch with

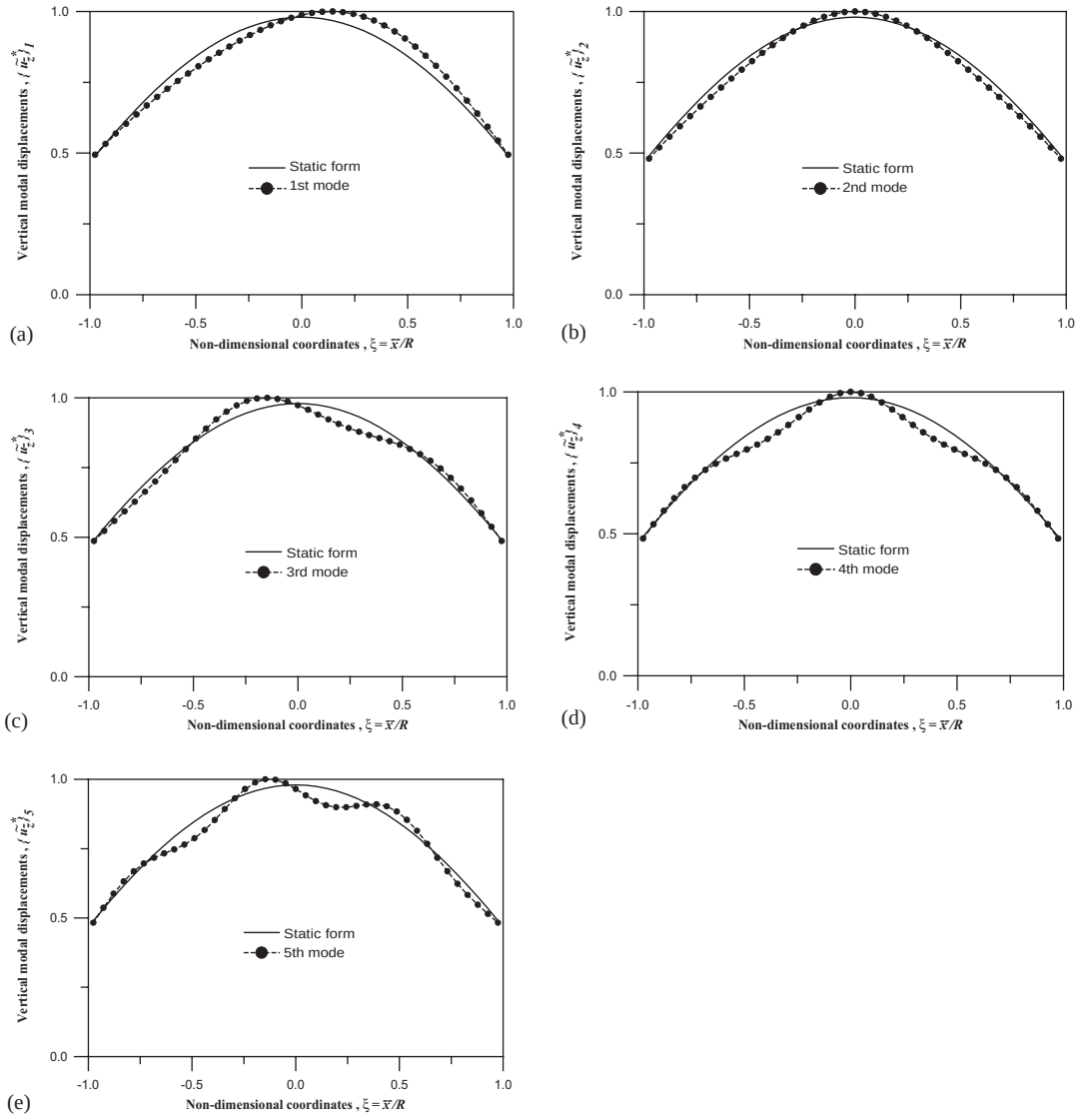

Fig. 14. The lowest five mode shapes of the *hinged–hinged* 120° circular arch (cf., Fig. 5).

"clamped–clamped" supports is much greater than that with "hinged–hinged" supports. It is evident that the magnification factor (D_i) will be meaningless if the associated static deflection ($\delta_{st\ i}$) is not given. For this reason, the values of the associated static deflections ($\delta_{st\ i}$) are shown in the captions of the relevant figures in this paper.

7.7. *Influence of moving speed on the maximum central bending moments*

Since the maximum bending moments induced by the maximum deflections at the relevant positions of a structural system are the important data for structural design, the influence of the

moving-load speed (V_P) on the maximum bending moments about the y-axis at the midpoints of the 120° arch and the hybrid beam, $\left|M_{yi}(t)\right|_{\max}$, was shown in Fig. 12. Where Fig. 12(a) is for the 120° arch with "clamped–clamped" supports and Fig. 12(b) is for the same arch with "hinged–hinged" supports, while Fig. 12(c) is for the hybrid beam with given data and supporting conditions shown in Fig. 9. The values of $\left|M_{yi}(t)\right|_{\max}$ shown in Fig. 12 were obtained from

$$\{\bar{F}\} = [\bar{K}]\ \{\bar{\delta}(t)\}_{\max}, \tag{47}$$

where $\{\bar{F}\}$ is the overall force vector, $[\bar{K}]$ is the overall stiffness matrix and $\{\bar{\delta}(t)\}_{\max}$ is the overall nodal displacement vector corresponding to the maximum vertical central displacement $|\delta_i(t)|_{\max}$. Comparing the curves of Figs. 12(a)–(c) with the corresponding solid curves shown in Figs. 7(b), 8(b) and 10(b), one sees that the trend for the maximum bending moments is the same as that for the maximum displacements as one may expect, because the bending moments are induced by the deflections.

8. Conclusions

1. For a uniform circular arch with constant curvature, the numerical values for the coefficients of the element stiffness matrix and those of the mass matrix are invariant if the subtended angle of each arch element is a constant. In addition, because the formulations are based on the polar co-ordinate system, transformation of each arch element matrix (from local co-ordinate system into global one) is not required before assembling. This is one of the main features that the arch element is superior to the straight-beam element for the dynamic analysis of the arches. Besides, for the same mesh density the accuracy of the arch element presented in this paper is much better than that of the conventional straight-beam element.
2. In theory, one may model an arch by a structural member composed of many straight-beam elements as precisely as possible by increasing the number and reducing the size of the straight-beam elements. However, the accuracy of the straight-beam elements is always worse than that of the arch elements.
3. For the first and second mode shapes of a circular arch with either clamped–clamped or hinged–hinged supports, their "crests" are near the position at $\frac{1}{4}$ (or $\frac{3}{4}$) of the arch length and their "nodes" are near the middle of the arch, therefore, when the circular arch is subjected to a load moving circumferentially, the maximum response occurs at the position near $\frac{1}{4}$ of the arch length. This is different from a clamped–clamped or hinged–hinged "straight beam subjected to a moving load, where the maximum response occurs at the middle of the straight beam.
4. The higher the moving-load speed the larger the centrifugal force, thus, the dynamic response of a circular arch due to a moving load decreases with increasing the moving-load speed. The frictional force has also the effect of reducing the dynamic response of an arch due to a moving load, but this effect is usually negligible.
5. If the finite element method (FEM) modelling both the straight-beam segments and the circular-arch segment with the straight-beam elements is called the S–S method, while that modelling the straight-beam segments with the straight-beam elements and the circular-arch segment with the curved-beam elements is called the S–C method, then, for the hybrid beam

subjected to a moving load, studied in this paper, the dynamic responses of the beam obtained from the S–S method are greater than the corresponding ones obtained from the S–C method.

Acknowledgements

This paper is part of the project under NSC89-2611-E-006-049, National Science Council, the Republic of China. The financial support of NSC is gratefully acknowledged.

References

[1] A.O. Lebeck, J.S. Knowlton, A finite element for the three-dimensional deformation for a circular ring, International Journal for Numerical Methods in Engineering 21 (1985) 421–435.
[2] R. Palaninathan, P.S. Chandrasekharan, Curved beam element stiffness matrix formulation, Computers and Structures 21 (4) (1985) 663–669.
[3] H.K. Stolarski, Y.M. Chiang, The mode-decomposition, C^0 formulation of curved, two-dimensional structural elements, International Journal for Numerical Methods in Engineering 28 (1989) 145–154.
[4] H.S. Ryu, H.C. Sin, Curved beam elements based on strained fields, Communications in Numerical Methods in Engineering 12 (1996) 767–773.
[5] P. Litewka, J. Rakowski, An efficient curved beam finite element, International Journal for Numerical Methods in Engineering 40 (1997) 2629–2652.
[6] P. Litewka, J. Rakowski, The exact thick arch finite element, Computers and Structures 68 (1998) 369–379.
[7] M. Petyt, C.C. Fleischer, Free vibration of a curved beam, Journal of Sound and Vibration 18 (1) (1971) 17–30.
[8] A.B. Sabir, D.G. Ashwell, A comparison of curved beam finite elements when used in vibration problem, Journal of Sound and Vibration 18 (4) (1971) 555–563.
[9] P. Litewka, J. Rakowski, Free vibration of shear-flexible and compressible arches by FEM, International Journal for Numerical Methods in Engineering 52 (2001) 273–286.
[10] Y.B. Yang, C.M. Wu, J.D. Yau, Dynamic Response of a horizontally curved beam subjected to vertical and horizontal moving loads, Journal of Sound and Vibration 242 (3) (2001) 519–537.
[11] J.S. Wu, L.K. Chiang, Free vibration analysis of arches using curved beam elements, International Journal for Numerical Methods in Engineering, accepted.
[12] J.S. Przemieniecki, Theory of Matrix Structural Analysis, McGraw-Hill, New York, 1968.
[13] K.J. Bathe, Finite Element Procedures in Engineering Analysis, Prentice-Hall, Englewood Cliffs, NJ, 1982.